Plastic Deformation and Ductility of AA7075 and AA6013 at Warm Temperatures Suitable to Retrogression Forming



KATHERINE E. RADER, JON T. CARTER, LOUIS G. HECTOR Jr., and ERIC M. TALEFF

A warm forming process with a simultaneous retrogression heat treatment, termed retrogression forming, can achieve good formability in high-strength aluminum alloys and recover their high strength through a single reaging heat treatment after forming. Tensile data from two commercial aluminum alloy sheet materials, AA7075-T6 and AA6013-T6, are presented for conditions suitable to retrogression forming. AA7075-T6 sheet was tested at temperatures from 180 °C to 220 °C and strain rates from 3.2×10^{-3} to 10^{-1} s⁻¹. AA6013-T6 sheet was tested from 230 °C to 250 °C and 3.2×10^{-3} to 10^{-1} s⁻¹. Both materials exhibit nearly steady-state flow at these temperatures and produce a modest strain-rate sensitivity of m = 0.039. The activation energies for plastic flow under these conditions are 221 kJ/mol for AA7075-T6 and 253 kJ/mol for AA6013-T6. Test data are used to construct predictive models for flow stress as a function of temperature and strain rate. AA7075-T6 demonstrates an excellent potential for retrogression forming at 200 °C and strain rates up to 10^{-1} s⁻¹ if time at temperature is held to under 12 minutes. AA6013-T6 exhibits a modest potential for retrogression forming at 240 °C and strain rates up to 10^{-1} s⁻¹ if time at temperature is held to under 7 minutes.

https://doi.org/10.1007/s11661-021-06360-z © The Minerals, Metals & Materials Society and ASM International 2021

I. INTRODUCTION

BECAUSE of their low density and high strength, high-strength aluminum alloys (HSAAs) are of interest to the automotive industry as lightweight material alternatives to the heavier ferrous alloys used in automotive structural applications. Alloy AA7075-T6, which was originally developed for aerospace applications, is of special interest for its high strength (YS≈ 505 MPa), but its quench sensitivity and susceptibility to stress corrosion cracking are potential concerns for automotive applications. AA6xxx-series aluminum alloy (YS≈ 320 MPa), is a potentially less expensive option that is less susceptible to stress corrosion cracking. One barrier to the implementation of HSAAs is their low ductility in the peak-aged T6 temper at room temperature. This limits the component geometries that can be formed in the T6 temper.

a stable soft temper condition that exhibits reasonable ductility exists, such as the T4 temper for AA6013, components might be formed at room temperature. [2,10-12,21,22] But these components must be subsequently aged to reach the high strength of the T6 temper, increasing production cost and potentially inducing warping of the formed component if the material must also be solution heat treated prior to aging. [2,10,11,21]

Elevated temperatures can significantly improve the formability of HSAAs by increasing ductility, decreasing the degree of springback, and reducing the forces necessary to form parts. [1-3,5-12,21,22] Elevated-temperature forming approaches can be categorized as warm forming or hot forming. Hot forming operations, typically conducted at temperatures ranging from 400 °C to 550 °C for aluminum alloys, significantly alter the temper condition of heat-treatable alloys. [2,5-7,11,21] Hot forming can also create significant material handling issues, particularly with part distortion and surface damage during handling and subsequent heat treating. [2,6,21] Warm forming of aluminum alloys at temperatures from approximately 200 °C to 300 °C can provide significantly improved ductility compared to room-temperature forming while avoiding some of the most serious problems associated with hot forming. [1,2,9-13,21, 22] However, warm forming may alter the

Manuscript submitted February 25, 2021; accepted June 9, 2021 Article published online July 8, 2021

KATHERINE E. RADER and ERIC M. TALEFF are with the The University of Texas at Austin, Department of Mechanical Engineering, Austin, TX 78712, USA. Contact e-mail: Kate.Rader@-utexas.edu. JON T. CARTER, LOUIS G. HECTOR, Jr. are with the Global Research and Development, General Motors, Warren, MI 48092, USA.

Jon T. Carter—(retired).

temper condition of the material. [2,9,10,12,13,22] For example, AA7075-T6 sheet exhibits improved formability in the vicinity of 200 °C, but exposure to this temperature can reduce the subsequent service strength of the material. [1,2,9-11,21] Previous published attempts to warm form HSAAs in the T6 condition primarily used trial-and-error to minimize strength loss during forming. [1,9,10,23] A new scientific approach to warm forming, termed retrogression forming and reaging (RFRA), was recently established to produce fully formed components of HSAAs with strengths equivalent to or exceeding those of the T6 temper. [13,24-30]

The RFRA process consists of two steps designed to improve the formability of precipitation-strengthened HSAAs while producing fully formed components with tensile strengths greater than or equal to those of the T6 temper. [13,24-30] During the first step, retrogression forming, material in a T6 temper is warm formed at a temperature that improves ductility and simultaneously induces a retrogression heat treatment. [13,24-29] The fully formed component can then be reaged to restore the strength of the T6 temper. [13,24-29] The reaging heat treatment might be partially or fully satisfied by the automotive paint-bake treatment in some cases. [13,24-30] Previous work by Park and Ardell identified the precipitate reactions that control retrogression and reaging of AA7075. [31] Previous work by the authors characterized retrogression and reaging behaviors in AA7075-T6 and AA6013-T6 with no plastic deformation. [24,25,30]

It is critically important to control temperature and time at elevated temperature during retrogression forming to ensure that a single reaging heat treatment can restore the original strength. To address this requirement, a retrogression forming window is defined using the first and second critical retrogression times, t_R^* and t_R^{max} , as defined in Figures 1. [29,30] Figure 1 presents schematics of typical RRA behaviors in (a) AA7075-T6 and (b) AA6013-T6. [24,25,30] The first critical retrogression time, t_R*, provides a useful target time for the retrogression forming process, although shorter times may also be used successfully. [29,30] The second critical retrogression time, $t_{\rm R}^{\rm max}$, is the absolute maximum time allowed for retrogression forming. [29,30] If retrogression forming exceeds this time limit, then a single reaging heat treatment cannot restore all the strength lost during retrogression forming. The retrogression forming window of AA7075-T6 at the recommended retrogression temperature of 200 °C is 3 to 12 minutes. [30] The retrogression forming window of AA6013-T6 at the recommended retrogression temperature of 240 °C is 6 to 8 minutes, although a total time at temperature of no longer than 7 minutes is recommended. [30] The authors previously recommended a reaging heat treatment of 120 °C for 24 hours for AA7075 and of 190 °C for 1 hour for AA6013. [24,25,30]

The present investigation was undertaken to characterize the tensile flow behaviors of AA7075 and AA6013 at conditions appropriate for retrogression forming. The warm temperatures, moderate true-strain rates, and times investigated represent conditions of interest for applying retrogression forming in commercial manufac-

turing. The data produced are analyzed to provide flow stress and ductility as functions of temperature and truestrain rate. Plastic flow data are analyzed to calculate the strain-rate sensitivity of the flow stress and the activation energy for plastic flow, which is physically distinct from the activation energy for retrogression. Strain-hardening behavior is also considered. The room-temperature deformation of both materials is studied through tensile tests for several temper conditions relevant to the RFRA process. The metallurgical mechanisms responsible for improved formability at the warm temperatures studied are considered. Table I lists the abbreviations and nomenclature used in this study.

II. EXPERIMENTAL PROCEDURES

Two commercial aluminum alloy sheet materials are studied: AA7075 (Al-Zn-Mg-Cu) and AA6013 (Al-Mg-Si-Cu). The nominal compositions of these alloys are listed by weight percent in Table II, according to their respective suppliers. [20,32] Both materials were received as sheet with a thickness of 2 mm. The AA7075 sheet material was received in the T6 temper, and the AA6013 sheet material was received in the T4 temper. Tensile specimens were machined from these sheets in the asreceived thickness. Two different specimen geometries were produced, one for room-temperature tensile experiments and the other for elevated-temperature tensile experiments. The geometry of the room-temperature tensile specimen, [33] and the geometry of the elevated-temperature tensile specimens is based on the ASTM E2448 tensile specimen. [34] All tensile specimens were produced by waterjet machining.

Room-temperature tensile specimens were produced from the as-received sheet materials with the tensile axes along the sheet rolling direction. The ASTM E8 subsize tensile geometry used has a gauge length of 25 mm (1 in) and a gauge width of 6 mm (0.25 in). Specimens of AA6013-T4 were solution heat treated at 570 °C for 1 hour, quenched in water, and then aged at 190 °C for 4 hours to produce the T6 temper. [20] Room-temperature tensile specimens of both alloys in the T6 condition were heat treated to produce the following additional conditions for tensile testing: a retrogressed condition (R), a retrogressed and paint-baked condition (RPB), and a retrogressed and reaged condition (RRA). These conditions and the heat treatments applied to produce each condition are described in Table III. [30] Heat treatments were conducted in preheated tube furnaces. Temperature was monitored with a type-K thermocouple in contact with the specimens during each heat treatment step. Temper condition was verified using Vickers hardness with a 10 kg load (HV₁₀) after each heat treatment. [35] All room-temperature tensile tests were conducted on a screw-driven universal testing machine under computerized control. Specimens were loaded in uniaxial tension until rupture at a constant engineering-strain rate of $\dot{e} = 0.01 \text{ s}^{-1}$. Engineering strain was measured using an extensometer with a 10 mm gauge length, and load was monitored with a

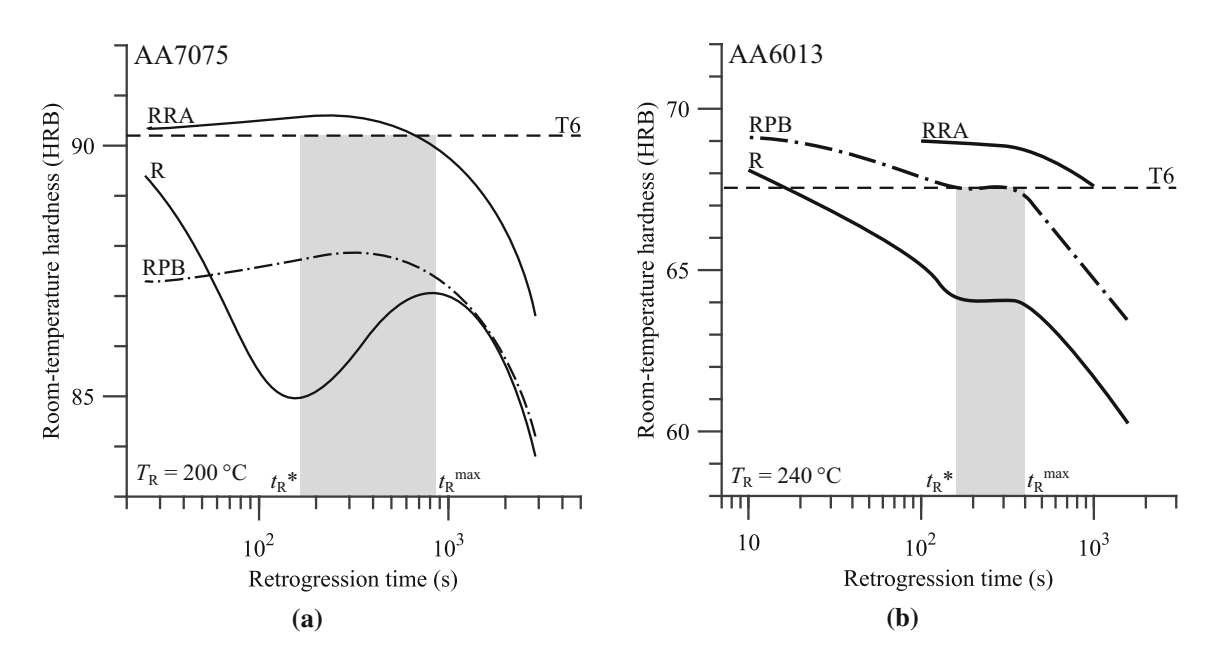


Fig. 1—Room-temperature hardness is plotted schematically as a function of retrogression time on a logarithmic scale for (a) AA7075 and (b) AA6013 subjected to retrogression alone (R) and for material reaged after retrogression (RRA) after the data from Ref. 30 Hardness after reaging with a simulated paint bake (RPB) is also shown. The mean original T6 hardnesses are represented by horizontal dashed lines. The critical retrogression times indicated are t_R^* and t_R^{max} .

Table I. Table of Nomenclature

Symbol	Description			
E	temperature-dependent dynamic unrelaxed Young's modulus			
ė	engineering-strain rate			
$e_{ m r}$	tensile elongation			
$\dot{arepsilon}$	true-strain rate			
$arepsilon_{\mathbf{P}}$	plastic true strain			
m	strain-rate sensitivity			
n	stress exponent			
$Q_{ m P}$	activation energy of plastic flow			
Q _R R	activation energy of retrogression			
R	universal gas constant			
R	retrogressed condition			
RA	reduction in area			
RPB	retrogressed and paint-baked condition			
RRA	retrogressed and reaged condition			
σ	flow stress			
σ_{05}	flow stress measured at a plastic true strain of 0.05			
σ_{10}	flow stress measured at a plastic true strain of 0.10			
5 ₁₅	flow stress measured at a plastic true strain of 0.15			
T	temperature			
$T_{ m m}$	melting temperature			
$T_{\mathbf{R}}$	retrogression temperature			
r * R max R	first critical retrogression time			
max R	second critical retrogression time			
T _R	reduced retrogression time			
${ au_{ m R}}^*$	first critical reduced retrogression time			
max R	second critical reduced retrogression time			
9	orientation of tensile axis relative to sheet rolling direction			
UTS	ultimate tensile strength			
YS	yield strength			
Z	Zener–Hollomon parameter			

load cell. Yield strength (YS) and ultimate tensile strength (UTS) were measured from engineering stress—strain data. Tensile elongation, $e_{\rm r}$, was measured after testing using the ASTM E8 procedure for elongation after fracture. [33,36] Reduction in area, RA, was calculated from measurements of the cross-sectional area at the location of specimen rupture using a caliper.

To produce AA6013 tensile specimens for elevatedtemperature experiments, four sheets of the as-received AA6013-T4 material with dimensions of $305 \times 305 \times$ 2 mm were heat treated to the T6 temper by solutionizing, quenching, and aging. Sheets were solutionized at 570 °C for 1 hour in a convection furnace, waterquenched, lightly rolled for flatness, and then aged to the T6 temper at 190 °C for 4 hours in a convection furnace. [20] Sheet temperature was monitored using type-K thermocouples clipped to the sheets. Elevatedtemperature tensile specimens of a slightly modified ASTM E2448 geometry were waterjet machined from the AA7075-T6 and AA6013-T6 sheets.^[34] The geometry of these specimens is shown in Figure 2. The only modification to the standard geometry is a slight shortening of the grip region height from 25 to 15 mm. Elevated-temperature tensile specimens were produced with three different orientations of the tensile axis relative to the sheet rolling direction (RD): $\theta = 0$, 45, and 90 deg, as shown in Figure 2.

Elevated-temperature tensile tests were conducted using a servo-hydraulic testing machine under computer control with a convection furnace mounted to its frame. The furnace and specimen grips were preheated to approximately 20 °C above the desired test temperature prior to specimen insertion to account for cooling during specimen insertion. Specimen insertion was accomplished in less than one minute to minimize heat loss. A small load of 44 N (10 lb) was applied to the specimen as it was heated in the grips. Specimens of AA7075 were tested at 180 °C, 200 °C, and 220 °C. Specimens of AA6013 were tested at 230 °C, 240 °C, and 250 °C. The recommendations of Reference 30 were used to select these warm temperatures for study. Two

type-K thermocouples, one in contact with each specimen grip region, monitored specimen temperature during testing. All specimens reached the desired test temperature in under 4 minutes 30 seconds. Once each specimen reached the desired test temperature, it was left to soak at temperature for a predetermined time, termed the *hold time*, prior to tensile straining. For specimens of AA7075, hold times from 20 to 900 seconds were investigated. Hold times longer than these are beyond the practical AA7075-T6 retrogression limits and, therefore, are not of interest for this study. [30] For all other tests of AA7075, the hold time was varied to maintain a constant reduced retrogression time of $\tau_R = 5 \times 10^{-9} \, \text{s}^{-1}$ prior to tensile deformation. Reduced time, τ_R , is defined as

$$\tau_{\rm R} = t_{\rm R} \times \exp\left(\frac{-Q_{\rm R}}{RT_{\rm R}}\right),$$
[1]

where t_R is retrogression time, Q_R is the activation energy of retrogression, R is the universal gas constant, and T_R is retrogression temperature in Kelvin. [13,24,25,28–30] The activation energies measured for retrogression are 97 ± 7 kJ/mol for AA7075-T6 and 160 ± 30 kJ/mol for AA6013-T6. For AA7075, the hold time at a test temperature of $T_R = 180$ °C was 420 seconds while the hold time at a test temperature of $T_R = 220$ °C was 60 seconds. For all AA6013 specimens, hold time was varied to maintain a constant reduced time of $\tau_R = 6 \times 10^{-15} \text{ s}^{-1}$ for every test. For example, the hold time at a test temperature of $T_R = 230$ °C was 360 seconds while the hold time at a test temperature of $T_{\rm R} = 250$ °C was 90 seconds. After reaching the test temperature and applying the desired hold time, if any, specimens were loaded in uniaxial tension until rupture at a constant true-strain rate. Specimen temperature was maintained to within ± 2 °C of the desired test temperature during tensile deformation. True-strain rates of $\dot{\varepsilon} = 3.2 \times 10^{-3}$, 10^{-2} , 3.2×10^{-2} , and 10^{-1} s⁻¹ were applied using computer control to vary piston displacement rate throughout each test, assuming conservation of volume

Table II. The Nominal Compositions of AA7075 and AA6013 in Weight Percent [16,32]

Alloy	Zn	Mg	Cu	Cr	Fe	Si	Mn	Ti	Al
AA7075	5.1 to 6.1	2.1 to 2.9	1.2 to 2.0	0.18 to 0.28	<0.5	<0.4	<0.3	<0.2	bal.
AA6013	≤0.25	0.8 to 1.2	0.6 to 1.1	≤0.1	≤0.5	0.6 to 1.0	0.2 to 0.8	≤0.1	bal.

Table III. Heat Treatment Conditions for This Study and Their Expected Vickers Hardness Values Based Upon Ref. [30]

Alloy	HT Condition	Heat Treatment Procedure	Expected Hardness (HV ₁₀) ^[32]
AA7075	R RPB	AA7075-T6→200 °C, 180 s+water-quench AA7075-R→185 °C, 25 min+water-quench	164±2 174±2
AA6013	RRA T6 R	AA7075-R \rightarrow 120 °C, 24 h+water-quench AA6013-T4 \rightarrow 570 °C, 1 h+water-quench \rightarrow 190 °C, 4 h+water-quench AA6013-T6 \rightarrow 240 °C, 400 s+water-quench	185 ± 2 127 ± 2 122 ± 2
	RPB RRA	AA6013-R \rightarrow 185 °C, 25 min+water-quench AA6013-R \rightarrow 190 °C, 1 h+water-quench	128 ± 2 128 ± 1

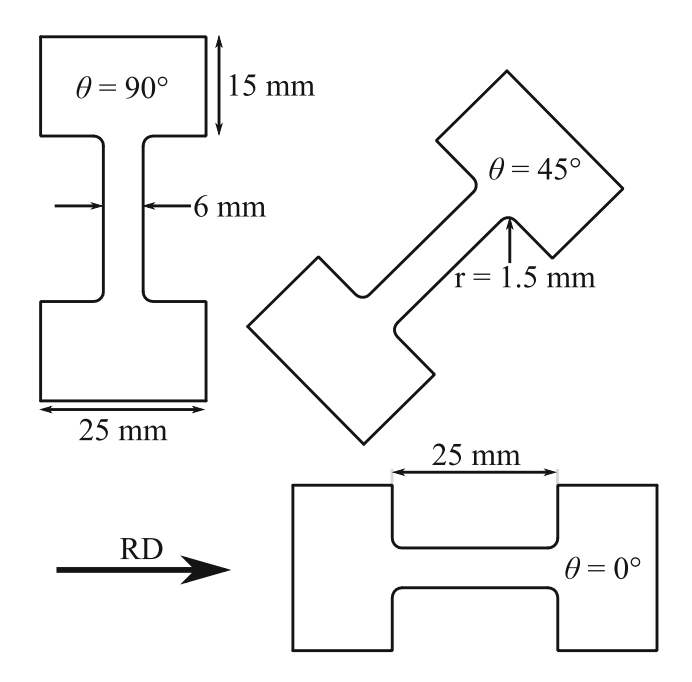


Fig. 2—The geometry of the specimens used for elevated-temperature tensile tests is shown with the three different orientations of specimens relative to the sheet rolling direction (RD). All dimensions are in mm.

and no necking in the specimen. Immediately after rupture, the specimen was quickly removed from the grips and quenched in water. Load was monitored using a load cell, and displacement was monitored from piston displacement using an LVDT (linear variable differential transformer). True stress and true strain were calculated from load-displacement data after correction for machine stiffness using the temperature-dependent dynamic unrelaxed Young's modulus of pure aluminum, E, expressed as a fit to the data of Köster. [14,37] The calculation of true stress and true strain assumed no necking, and this assumption was checked against the geometry of tested specimens to determine the extent of its validity. Flow stress was measured at designated plastic true strains of $\varepsilon_P = 0.05$, 0.10, and 0.15. Tensile elongation, e_r , was measured according to the ASTM E8 procedure for measuring elongation after fracture. [33,36] Reduction in area, RA, was calculated from measurements of cross-sectional area at the location of rupture using a caliper.

III. RESULTS

A. Room-Temperature Tensile Tests

Figure 3 presents examples of engineering stress-strain data at room temperature for the (a) AA7075 and (b) AA6013 materials in the heat-treated conditions described in Table III. Table IV lists the number of specimens tested at room temperature for each heat-treated condition and the average yield strength (YS), ultimate tensile strength (UTS), tensile elongation (e_T), and reduction in area (RA) for each condition. Minimum

and maximum values are listed in parentheses for each condition as a measure of uncertainty. For AA7075-T6, the recommended retrogression heat treatment is 200 °C for 180 seconds. [30] This retrogression heat treatment reduces the room-temperature YS and UTS of AA7075 by 12 and 9 pct, respectively, from those of the original T6 temper. The recommended retrogression heat treatment increases e_r and RA to 1.06 and 1.26 times those of the original T6 temper. Reaging AA7075 with a simulated paint-bake heat treatment of 185 °C for 25 minutes^[13] after the recommended retrogression heat treatment increases YS and UTS to 91 and 93 pct of those of the original T6 temper, respectively. For AA7075, the simulated paint-bake heat treatment is not as effective as the recommended reaging heat treatment, 120 °C for 24 hours. [30] This recommended reaging heat treatment for AA7075 fully restores both YS and UTS to those of the original T6 temper.

For AA6013, the T6 temper has a YS that is 57 pct greater than the T4 temper. However, the T4 temper strain hardens considerably, and the UTS of the T6 temper is only 13 pct greater than that of the T4 temper. The T6 temper is less ductile than the T4 temper, with an average $e_{\rm r}$ that is approximately one-half that of the T4 temper. RA for the T4 temper is only slightly greater than RA for the T6 temper. For AA6013-T6, the recommended retrogression heat treatment is 240 °C for 400 s. [30] After this retrogression heat treatment, there is no significant change in YS, e_r , or RA, and UTS is reduced by a slight 3 pct. The changes in YS, e_r , and RA from the original T6 temper to the R condition are less than their respective measurement uncertainties. For AA6013, the changes in YS, UTS, e_r , and RA from reaging with a simulated paint-bake heat treatment of 185 °C for 25 minutes^[13,24,25,28–30,38–40] are less than their respective measurement uncertainties. The recommended reaging heat treatment for AA6013 is 190 °C for 1 hour. [30] For AA6013, the changes in YS, UTS, e_r , and RA after reaging with the recommended reaging heat treatment are also less than their respective measurement uncertainties. These results differ somewhat from those of hardness tests previously performed for AA6013 by the authors. [30] The hardness testing demonstrated measurable differences in hardness between the different heat-treated conditions. The slightly different findings of the present tensile tests compared to the previous hardness tests are thought to be a result of greater variation in the heat treatments applied to tensile coupons, which used tube and box furnaces, compared to the more controlled heat treatments applied to hardness specimens, which primarily used salt pots. [30]

B. Elevated-Temperature Tensile Tests

Table V lists the combinations of elevated temperature (T), true-strain rate $(\dot{\epsilon})$, and specimen orientation (θ) studied for each material. All tests at elevated temperatures used material initially in a T6 temper. The number of tests performed at each set of test conditions is listed with the average values of true flow stress measured at various plastic true strains $(\varepsilon_{\rm P}=0.05$ for

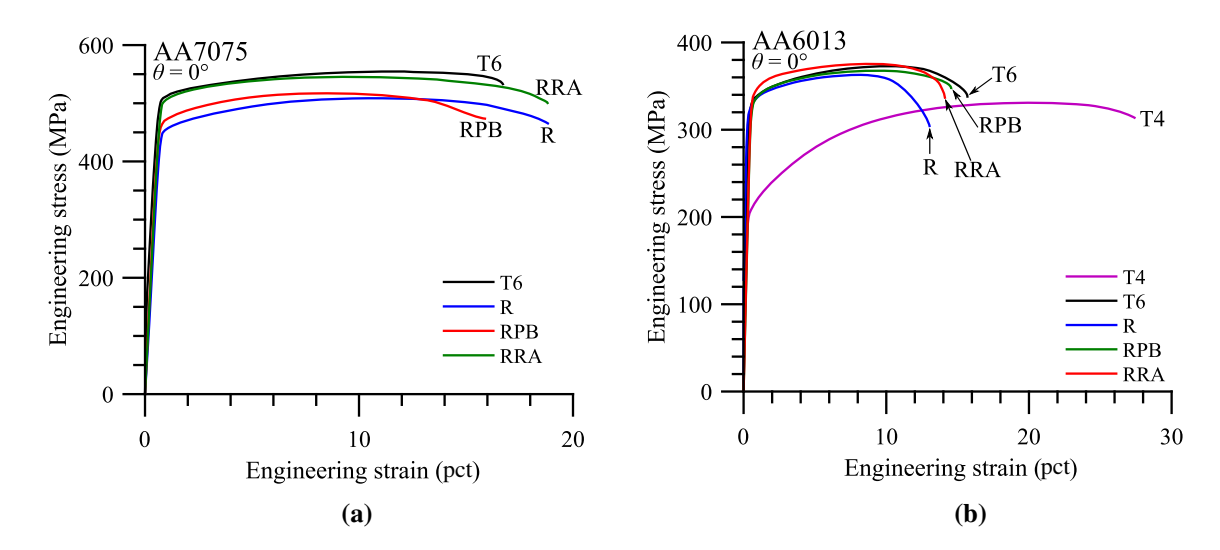


Fig. 3—Representative engineering stress–strain data are shown for (a) AA7075 and (b) AA6013 at room temperature in several different heat-treated conditions. Following the recommended retrogression heat treatment with the recommended reaging heat treatment fully restores strength.

Table IV. Average Yield Strength (YS), Ultimate Tensile Strength (UTS), Tensile Elongation (e_r), and Reduction in Area (RA) of AA7075 and AA6013 at Room Temperature in the Various Heat-Treated Conditions with Minimum and Maximum Values Listed in Parentheses

Alloy	HT Condition	# Of Tests	YS (MPa)	UTS (MPa)	$e_{\rm r}$ (Percent)	RA (Percent)
7075	T6	5	511 (500, 525)	556 (552, 564)	13 (12, 14)	22 (18, 27)
	R	5	449 (441, 461)	507 (504, 509)	14 (13, 15)	28 (26, 30)
	RPB	10	466 (458, 475)	517 (509, 521)	13 (12, 14)	30. (25, 34)
	RRA	10	509 (499, 516)	547 (540, 553)	13 (12, 13)	20. (11, 26)
6013	T4	4	210. (202, 220.)	331 (328, 336)	26 (26, 26)	31 (29, 34)
	T6	5	330. (320., 344)	374 (369, 379)	14 (13, 16)	28 (26, 31)
	R	6	328 (316, 335)	362 (356, 367)	13 (13, 14)	29 (26, 36)
	RPB	7	330. (325, 336)	367 (359, 373)	13 (12, 14)	30. (23, 35)
	RRA	7	335 (325, 348)	368 (360., 375)	12 (11, 14)	28 (25, 35)

 σ_{05} , 0.10 for σ_{10} , and 0.15 for σ_{15}), tensile elongation (e_r), and reduction in area (RA) for each set of test conditions. For tests without σ_{15} values, true flow stress could not be accurately measured at a plastic true strain of 0.15 because of early necking. Where multiple tests are available, ±half the maximum difference among the measured values is provided as a quantification of uncertainty. Examples of engineering stress-strain data for AA7075-T6 and AA6013-T6 at elevated temperatures are presented in Figure 4. Figures 4(a), (c), and (e) present data for AA7075. Figures 4(b), (d), and (f) present data for AA6013. Figures 4(a) and (b) demonstrate the effect of temperature. For both AA7075 and AA6013, flow stress decreases as temperature increases. Figures 4(c) and (d) demonstrate the effect of true-strain rate. For both AA7075 and AA6013, flow stress increases as true-strain rate increases, indicating that both materials are strain-rate sensitive at these temperatures. For AA7075, tensile elongation increases as truestrain rate decreases, suggesting that ductility may be sensitive to strain rate. Figures 4(e) and (f) demonstrate the effect of tensile axis orientation relative to the sheet rolling direction. For both AA7075 and AA6013, tensile axis orientation relative to the sheet rolling direction has no consistent effect on flow stress at elevated temperature.

Examples of true stress-strain data for AA7075-T6 and AA6013-T6 at different temperatures are presented in Figures 5(a) and (b), respectively. True stress-strain data are shown up to a true strain of 0.15. At elevated temperatures, both AA7075 and AA6013 demonstrate a nearly steady-state true flow stress at constant temperature and a constant true-strain rate across these strains. Slight decreases in flow stress as true strain increases are most likely artifacts of necking, which violates the assumption of prismatic geometry used to calculate true values for stress and strain. This effect is small and considered negligible for the data analysis conducted here. The strain-hardening exponents of 0.03 ± 0.01 for AA7075-T6 and 0.01 ± 0.01 for AA6013 are negligible at these elevated temperatures.^[41] At room temperature, both AA7075-T6 and AA6013-T6 present small strainhardening exponents of approximately 0.08 ± 0.00 . AA6013-T4 strain hardens substantially at room temperature with a strain-hardening exponent 0.21 ± 0.01 .

Table V. Average Tensile Properties Measured by Alloy, Orientation (θ), Temperature (T), and True-Strain Rate ($\hat{\epsilon}$); see Table I for Definitions of Symbols

Alloy	θ (°)	<i>T</i> (°C)	ἐ (1/s)	# Of Tests	$\sigma_{05} \; (MPa)$	$\sigma_{10} \; (MPa)$	$\sigma_{15} \; (MPa)$	$e_{\rm r}$ (Percent)	RA (Percent)
7075	0	180	0.0032	2	392±2	404±2	410±2	33±1	46±2
			0.01	2	401 ± 3	411 ± 7	399 ± 24	26 ± 3	40 ± 4
			0.032	2	417 ± 1	428 ± 2	428 ± 2	24 ± 0	42 ± 2
			0.1	2	435 ± 2	445 ± 2	433 ± 2	22 ± 1	37 ± 1
		200	0.0032	2 2 2	352 ± 2	358 ± 1	355 ± 1	33 ± 2	46 ± 1
			0.01	2	366 ± 1	374 ± 1	374 ± 1	31 ± 0	45 ± 2
			0.032	2 2	382 ± 3	389 ± 3	385 ± 3	26 ± 0	38 ± 3
			0.1	2	398 ± 2	402 ± 2	391 ± 2	23 ± 1	41 ± 2
		220	0.0032	2	316 ± 0	310 ± 0	_	29 ± 0	44 ± 3
			0.01	3	338 ± 2	338 ± 2	331 ± 2	29 ± 1	44 ± 1
			0.032	2	346 ± 5	342 ± 10	_	23 ± 3	40 ± 2
			0.1	2	369 ± 2	370 ± 2	356 ± 3	25 ± 1	44 ± 4
	45	180	0.0032	2	381 ± 1	392 ± 1	397 ± 1	30 ± 1	44 ± 1
			0.1	2	438 ± 1	447 ± 2	432 ± 5	22 ± 0	39 ± 1
		200	0.0032		352 ± 1	359 ± 0	357 ± 0	29 ± 0	44 ± 2
			0.1	2 2 2	401 ± 3	407 ± 3	396 ± 3	23 ± 0	38 ± 1
		220	0.0032	2	316 ± 2	310 ± 2	_	30 ± 1	45 ± 1
			0.1	2	364 ± 2	364 ± 2	_	23 ± 0	40 ± 4
	90	180	0.0032	2	389 ± 4	400 ± 4	403 ± 4	30 ± 1	45 ± 3
			0.1	2	436 ± 7	445 ± 7	429 ± 8	22 ± 0	39 ± 1
		200	0.0032	2	358 ± 3	363 ± 2	360 ± 2	29±1	44±4
			0.1	1	415	421	405	22	40
		220	0.0032	2	325 ± 1	318 ± 0	_	29 ± 3	47 ± 1
			0.1	2	380 ± 4	379 ± 4	_	22 ± 0	42±1
6013	0	230	0.0032	2	267 ± 3	268 ± 2	_	24 ± 3	39 ± 0
			0.01	2 2 2 2	278 ± 1	280 ± 2	_	22 ± 2	38 ± 0
			0.032	2	287 ± 0	289 ± 1	280 ± 7	24 ± 2	41 ± 1
			0.1	2	299 ± 1	300 ± 1	_	20 ± 1	35 ± 1
		240	0.0032	2	249 ± 5	248 ± 7	_	21 ± 0	34 ± 2
			0.01	2	265 ± 1	266 ± 1	_	21 ± 1	41 ± 3
			0.032	2	279 ± 1	278 ± 1	_	21 ± 2	38±1
			0.1	2	285 ± 1	286 ± 1	276 ± 2	22 ± 1	42 ± 1
		250	0.0032	2	241 ± 2	239 ± 2	_	21 ± 1	38 ± 2
			0.01	1	252	253	250	29	41
			0.032	2	262 ± 0	263 ± 1	254 ± 1	24 ± 0	40±3
			0.1		274 ± 1	275 ± 1	261 ± 4	23 ± 2	39±1
	45	230	0.0032	2 2 2 2	269 ± 1	271 ± 0	266 ± 0	24 ± 0	37 ± 3
		200	0.1	2	306 ± 1	310 ± 1	303 ± 1	22 ± 1	38 ± 1
		240	0.0032	2	263 ± 7	263 ± 8	_	23 ± 1	35 ± 1
		2.0	0.1	2	288 ± 3	289 ± 4	_	20 ± 1	38 ± 2
		250	0.0032	2	238 ± 2	237 ± 2	227 ± 1	22 ± 1	39 ± 4
		230	0.1	2	277 ± 3	277 ± 3	_	20 ± 1	37 ± 0
	90	230	0.0032	2	268 ± 3	268 ± 6	_	20 ± 1	44 ± 3
	70	230	0.0032	2	298 ± 3	301 ± 4	_	20 ± 1 22 ± 2	40 ± 3
		240	0.0032	4	254 ± 6	244 ± 2	_	19 ± 4	46 ± 4
		210	0.0032	4	290 ± 4	_	_	18±4	40 ± 7
		250	0.0032	2	242 ± 3	240 ± 4	_	21 ± 1	33 ± 3
		230	0.0032	2	272 ± 8	2 4 0± 4	_	20 ± 2	36 ± 1
			0.1	4	4/410			2012	JU 1 1

The effects of hold time at temperature prior to tensile straining were considered for AA7075. Figure 6 presents true flow stress for AA7075 at a plastic true strain of 0.10, σ_{10} , plotted against hold time on a logarithmic scale. For the range of hold times studied, there is no effect of hold time on true flow stress. Data from these same tests demonstrate that hold time does not significantly affect e_r or RA values either. However, it should be remembered that retrogression time determines the ability to restore T6 strength by reaging following retrogression. Retrogression for a time that exceeds $t_R^{\rm max}$

will result in an unrecoverable loss of strength that a single reaging heat treatment may not restore. For AA7075, this is because the solute elements necessary to form a fine dispersion of strengthening precipitates are consumed by coarse precipitates.^[31]

True flow stress in AA7075 at a plastic true strain of 0.10 (σ_{10}) is plotted as a function of true-strain rate in Figure 7 on dual-logarithmic scales. These data are for temperatures of 180 °C, 200 °C, and 220 °C and the $\theta = 0$ deg specimen orientation. The mean YS of the T6 temper at room temperature (511 \pm 12 MPa) is

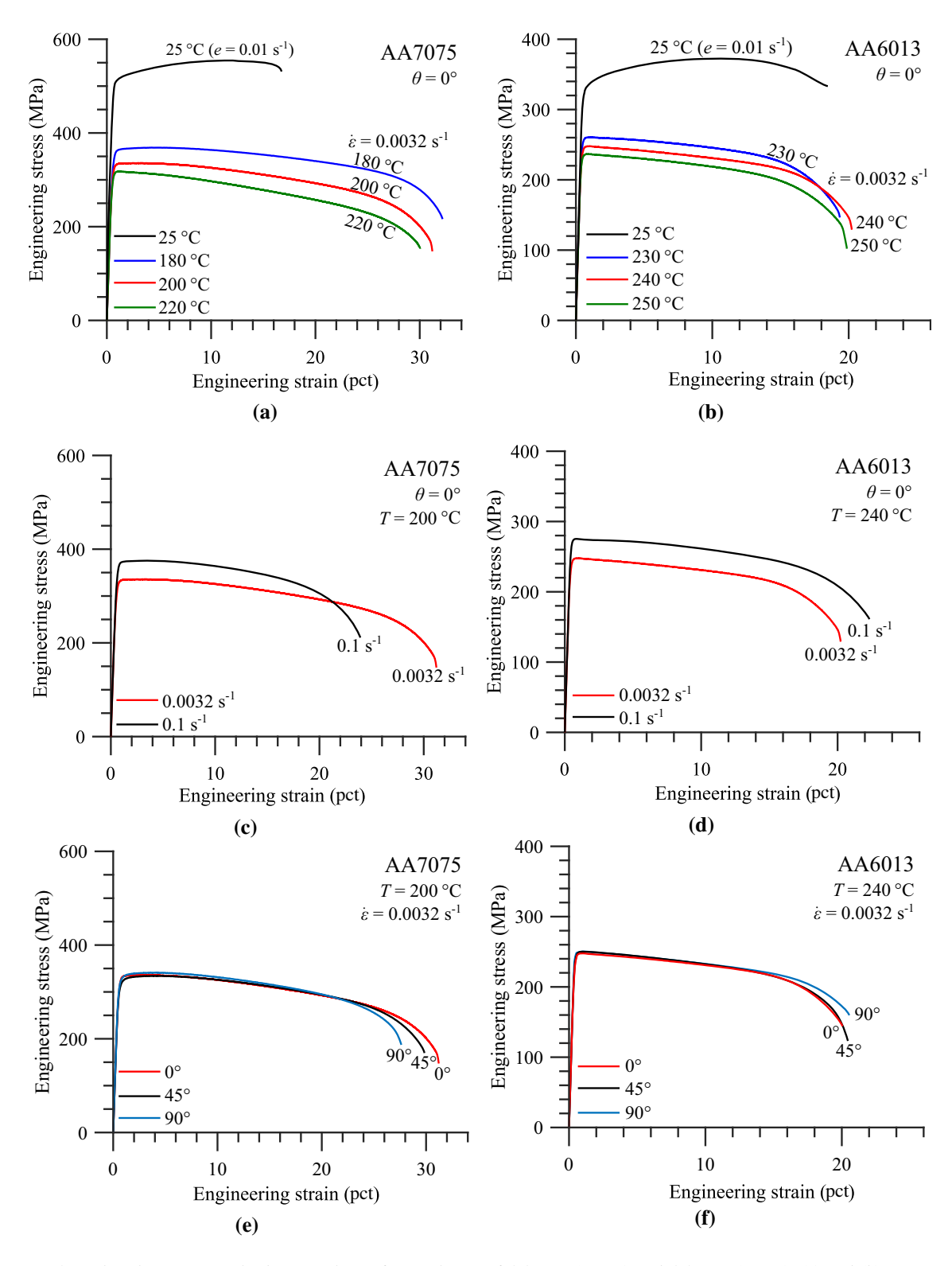


Fig. 4—Example engineering stress–strain data are shown for specimens of AA7075 (a, c, e) and AA6013 (b, d, f). (a) and (b) compare the tensile behaviors of AA7075 and AA6013 at elevated temperatures to those of their respective T6 tempers at room temperature. (c) and (d) compare the tensile behaviors of AA7075 and AA6013 at different true-strain rates. (e) and (f) compare the tensile behaviors of AA7075 and AA6013 at different orientations of the tensile axis relative to the sheet rolling direction; see Figure 2.

indicated by a horizontal dashed line. While this mean YS is measured from engineering stress—strain data, the difference between engineering stress and true stress at

the point of yielding is negligible. True flow stresses at elevated temperatures are 10 to 40 pct less than the mean room-temperature YS of the T6 temper. The slope of the

data in Figure 7 is equal to the strain-rate sensitivity, m. The average m measured across all elevated-temperature test conditions for AA7075 is 0.039. The strain-rate sensitivity varies little with temperature from 180 °C to 220 °C or with true-strain rate from 3.2×10^{-3} to 10^{-1} s⁻¹

True flow stress in AA6013 at a plastic true strain of 0.10 (σ_{10}) is plotted as a function of true-strain rate in Figure 8 on dual-logarithmic scales. These data are for temperatures of 230 °C, 240 °C, and 250 °C and the $\theta = 0$ deg specimen orientation. The mean YS values of the T4 and T6 tempers at room temperature (210 \pm 9 MPa and 330 ± 12 MPa, respectively) are indicated by horizontal dashed lines. While these mean YS values are measured from engineering stress-strain data, the difference between engineering stress and true stress at the point of yielding is negligible. The true flow stresses in AA6013 at elevated temperature are 10 to 30 pct less than the mean room-temperature YS of the T6 temper but are consistently greater than the mean roomtemperature YS of the T4 temper. The T4 temper, however, exhibits significant strain hardening at room temperature, as shown in Figure 5(b). The average true flow stress in AA6013-T4 at room temperature for a plastic true strain of 0.10 (σ_{10}) is 352 \pm 6 MPa, which is 17 to 47 pct greater than σ_{10} for AA6013-T6 at the elevated temperatures studied. The slope of the data in Figure 8 is equal to the strain-rate sensitivity, m. The average m measured across all elevated-temperature test conditions for AA6013 is 0.039, the same as that measured for AA7075, and does not vary significantly with temperature from 230 °C to 250 °C or with truestrain rate from 3.2×10^{-3} to 10^{-1} s⁻¹. The similarity in strain rate sensitivities between the AA6013 and AA7075 materials may be simply coincidental.

The effects of temperature and true-strain rate on two measures of ductility, tensile elongation (e_r) and reduction in area (RA), are presented in Figure 9 for AA7075. In Figure 9(a), e_r for AA7075 is plotted as a function of true-strain rate on a logarithmic scale for specimens tested at 180 °C, 200 °C, and 220 °C with the $\theta = 0$ deg specimen orientation. The values of e_r decrease steadily with increasing strain rate, but there is no dependence of $e_{\rm r}$ on test temperature. The average value of $e_{\rm r}$ at the slowest true-strain rate, 3.2×10^{-3} s⁻¹, is 32 pct. This is 2.5 times that of the T6 temper at room temperature, 13 pct. The average value of e_r at the fasted true-strain rate, 10^{-1} s⁻¹, is 23 pct. This is 1.8 times that of the T6 temper at room temperature. In Figure 9(b), RA for AA7075 is plotted as a function of true-strain rate on a logarithmic scale for specimens tested at 180 °C, 200 °C, and 220 °C with the $\theta = 0$ deg specimen orientation. There is no dependence of RA on temperature except at the fastest strain rate, 10^{-1} s⁻¹, for which RA increases from 37 pct at 180 °C to 44 pct at 220 °C. The average value of RA across all temperatures at 10^{-1} s⁻¹ is 41 pct, which is 1.9 times that of the T6 temper at room temperature, 22 pct. For the other strain rates studied, RA increases as true-strain rate decreases from 3.2×10^{-2} s^{-1} to 3.2×10^{-3} s⁻¹. The average value of *RA* at the slowest true-strain rate studied, 3.2×10^{-3} s⁻¹, is 46 pct,

which is 2.1 times that of the T6 temper at room temperature.

The effects of temperature and true-strain rate on two measures of ductility, e_r and RA, are shown in Figure 10 for AA6013. In Figure 10(a), e_r in AA6013 is plotted as a function of true-strain rate on a logarithmic scale for specimens tested at 230 °C, 240 °C, and 250 °C with the $\theta = 0$ deg specimen orientation. There is no dependence of e_r on temperature. The values of e_r vary slightly with strain rate, but these variations are generally smaller than the scatter in the data. The average $e_{\rm r}$ across all strain rates and elevated temperatures studied is 23 pct, which is 1.6 times that of the T6 temper at room temperature, 14 pct, and is 0.9 times that of the T4 temper at room temperature, 26 pct. While the e_r values at the elevated temperatures studied are less than that of the T4 temper at room temperature, they are substantially greater than that of the T6 temper at room temperature. In Figure 10(b), RA in AA6013 is plotted as a function of true-strain rate on a logarithmic scale for specimens tested at 230 °C, 240 °C, and 250 °C with the $\theta = 0$ deg specimen orientation. RA does not vary with temperature but does change with true-strain rate. RA slightly increases as true-strain rate increases from $3.2 \times$ 10^{-3} s⁻¹ to 10^{-2} s⁻¹ and then slightly decreases as truestrain rate increases from 10^{-2} s⁻¹ to 10^{-1} s⁻¹. The smallest RA measured is 32 pct at T = 240 °C and $\dot{\varepsilon} =$ 3.2×10^{-3} s⁻¹. The largest RA measured is 44 pct at T = 240 °C and $\dot{\varepsilon} = 10^{-2}$ s⁻¹. The average RA at the fastest true-strain rate studied, 10^{-1} s⁻¹, is 39 pct, which is 1.4 times that of the T6 temper at room temperature, 28 pct, and is 1.3 times that of the T4 temper at room temperature, 31 pct.

A statistical analysis of the data obtained at elevated temperatures was used to determine the effects of tensile axis orientation relative to the sheet rolling direction (θ) on flow stress (σ_{10}), tensile elongation (e_r), and reduction in area (RA). Ninety-five percent simultaneous observation prediction bounds were calculated for σ_{10} , e_r , and RA at the $\theta = 0$ deg specimen orientation as functions of true-strain rate for each temperature studied. The MATLABTM 'predint' software function was used for these calculations.^[42] Data from other specimen orientations were then compared to the 95 deg prediction bounds of the $\theta = 0$ deg specimen orientation to evaluate the effect of specimen orientation. Simultaneous observation bounds account for the uncertainty of data from the $\theta = 0$ deg specimen orientation and the random variation of each new observation across all strain rates. [42] If 95 pct of the data from the $\theta = 45$ and 90 deg orientations are within the 95 pct prediction bounds determined from the 0 deg orientation, then specimen orientation does not produce a statistically significant difference in the measured quantity. For the AA7075 material, specimen orientation does not produce any statistically significant effect on σ_{10} or RA. Of the e_r data for the $\theta = 45$ and 90 deg orientations, only 83 pct are within the 95 pct prediction bounds. The e_r data outside of the prediction bounds for both the 45 and 90 deg orientations are strictly from specimens tested at T = 200 °C and $\dot{\varepsilon} = 3.2 \times 10^{-3}$ s⁻¹. Thus, if specimen orientation has any effect on e_r in AA7075, it is quite limited.

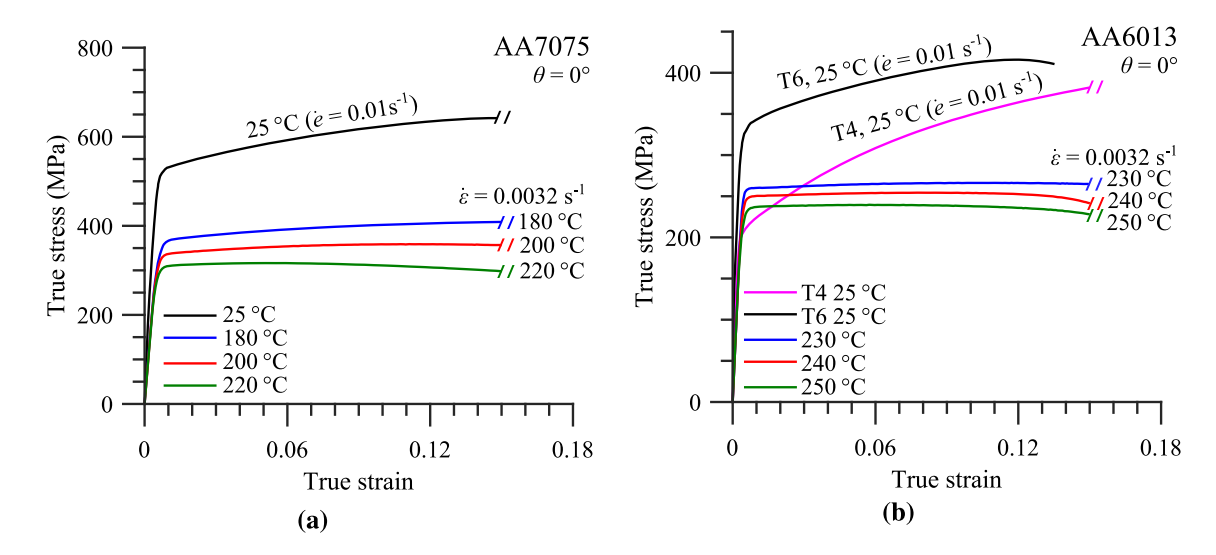


Fig. 5—Example true stress–strain data are shown for (a) AA7075 and (b) AA6013 up to a true strain of 0.15. (a) compares data from AA7075-T6 at room temperature and three elevated temperatures. (b) compares data from AA6013-T4 and AA6013-T6 at room temperature and AA6013-T6 at three elevated temperatures.

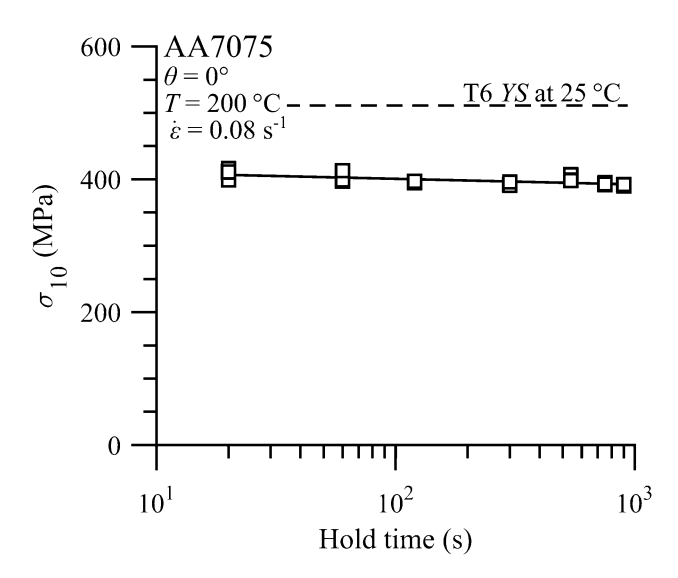


Fig. 6—Flow stress measured at a plastic true strain of 0.10 (σ_{10}) is plotted as a function of hold time at 200 °C prior to tensile testing on a logarithmic scale for specimens of AA7075 in the $\theta=0$ deg orientation. Specimens were tested at a constant true-strain rate of $8\times 10^{-2}~\rm s^{-1}$. Three tests were conducted for each hold time. The yield strength of the T6 condition at room temperature is indicated by a horizontal dashed line.

For the AA6013 material, specimen orientation does not produce any statistically significant effect on σ_{10} , e_r , or RA.

IV. DISCUSSION

Because the true flow stress data from both AA7075 and AA6013 at elevated temperatures demonstrate a nearly steady-state true stress at constant temperature and constant true-strain rate across significant strains, as shown in Figure 5, a steady-state analysis of these

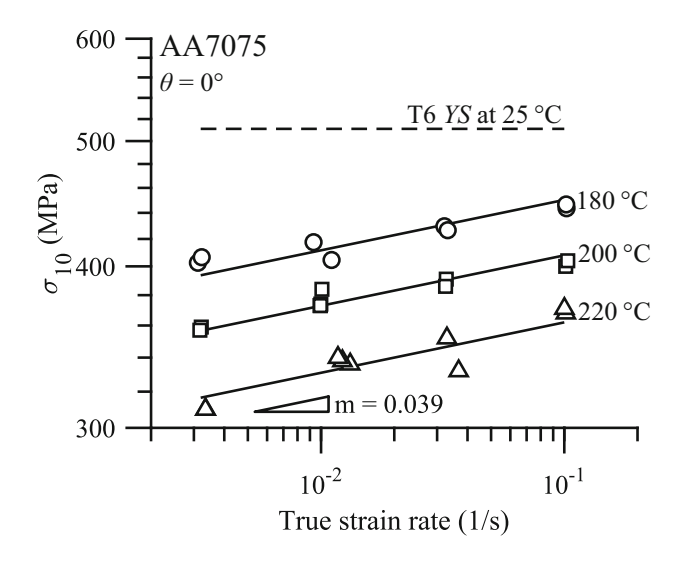


Fig. 7—Flow stress measured at a plastic true strain of $0.10~(\sigma_{10})$ is plotted as a function of constant true-strain rate on dual-logarithmic scales for specimens of AA7075 in the $\theta=0$ deg orientation. Specimens were tested at 180 °C, 200 °C, and 220 °C. Strain rate sensitivity, m, is the slope of the data. The yield strength of the T6 condition at room temperature is indicated by a horizontal dashed line

data is pursued. The activation energies of plastic flow at the temperatures and true-strain rates studied are determined using the phenomenological equation for steady-state creep, [14,43,44]

$$\dot{\varepsilon} = A \left(\frac{\sigma}{E}\right)^n \exp\left(\frac{-Q_{\rm P}}{RT}\right),\tag{2}$$

where $\dot{\varepsilon}$ is the true-strain rate, A is a material constant, σ is true flow stress, E is the temperature-dependent dynamic unrelaxed Young's modulus, n is the stress exponent, Q_P is the activation energy of plastic flow, R is the universal gas constant, and T is temperature in

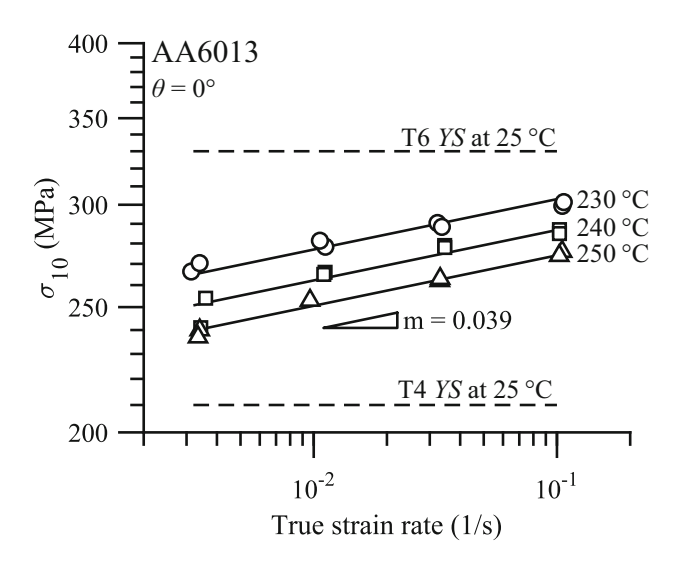


Fig. 8—Flow stress measured at a plastic true strain of 0.10 (σ_{10}) is plotted as a function of constant true-strain rate on dual-logarithmic scales for specimens of AA6013 in the $\theta=0^{\circ}$ orientation. Specimens were tested at 230 °C, 240 °C, and 250 °C. The strain rate sensitivity, $m_{\rm c}$ is the slope of the data. The yield strength of the T6 and T4 conditions at room temperature are indicated by horizontal dashed lines.

Kelvin. Taking data at a constant σ/E enables calculation of the activation energy for plastic flow as follows:

$$\left. \frac{d\ln(\dot{\varepsilon})}{d1/T} \right|_{\sigma/E} = -\frac{Q_{\rm P}}{R}.$$
 [3]

The fits to data shown in Figures 7 and 8 are used with the temperature-dependent dynamic unrelaxed Young's modulus values for pure aluminum from Köster^[14,37] to calculate true-strain rate at a constant value of σ/E for each test temperature. In Figure 11, $\dot{\epsilon}$ is plotted against 1/T on dual-logarithmic scales at the constant σ/E values of 5.8×10^{-3} for AA7075 and 4.3×10^{-3} for AA6013. The slope of the data in Figure 11 equals $-Q_P/R$ for each material. The activation energy for plastic flow in AA7075 is measured as 221 kJ/mol, and the activation energy for plastic flow in AA6013 is measured as 253 kJ/mol. These activation energies are larger than the activation energies for self-diffusion and for steady-state creep controlled by dislocation climb in aluminum, approximately 140 to 150 kJ/mol.[14,45-47] The activation energies for plastic flow are also quite different from the activation energies previously measured for retrogression, as expected for physically distinct phenomena. [30] These results suggest that the mechanisms controlling plastic flow at these warm temperatures and moderate strain rates are more complex than the classical creep mechanisms that control deformation at higher temperatures and slower strain rates. This interpretation is supported by the strain-rate sensitivity measured from these data, m = 1/n = 0.039, which is approximately five times smaller than those observed for steady-state creep deformation, typically dislocation climb from $m \approx 0.2$ for controlled

creep. [14,45,47,48] It is somewhat surprising that a nearly steady-state true flow stress is observed at the temperatures and strain rates investigated, although a steady-state flow stress was observed at similar conditions for AA7075 by other authors. [10,49,50] Current plastic deformation theory does not yet provide a clear mechanistic explanation for this observation.

The Zener–Hollomon parameter provides a useful means of relating the true-strain rate of tensile deformation with temperature for plastic flow at elevated temperatures. [45,46,51] The Zener–Hollomon parameter^[51] is

$$Z = \dot{\varepsilon} \exp\left(\frac{Q_P}{RT}\right),$$
 [4]

where Q_P is the activation energy for plastic flow measured using a steady-state analysis of flow stress. The Zener-Hollomon parameter is applied to relate the true flow stresses measured for AA7075 and AA6013 to temperature and true-strain rate. True flow stress measured at a plastic true strain of 0.10 and normalized by the temperature-dependent dynamic unrelaxed Young's modulus (σ_{10}/E) is plotted against the Zener-Hollomon parameter (Z) on dual-logarithmic scales in Figure 12(a) for AA7075 and in Figure 12(b) for AA6013. The slope of the data equals the strain-rate sensitivity, m = 0.039, which is the same for both AA7075 and AA6013. True flow stress in uniaxial tension can be estimated as a function of temperature and true-strain rate using the following equation fit to the data of Figure 12:

$$\frac{\sigma_{10}}{F} = BZ^m, ag{5}$$

where $B = (1/A)^m$ and m = 1/n from Eq. [2]. B is a material-dependent constant. Taking Z in units of 1/s, B equals 7.7×10^{-4} s⁻¹ for AA7075-T6 and 5.0×10^{-4} s⁻¹ for AA6013-T6.

The goal of RFRA is to improve the formability of material in the T6 temper while ultimately producing fully formed components with strengths equal to or greater than those of the original T6 temper. Improved formability is expected to result from reduced true flow stress, increased tensile elongation, and increased reduction in area. Retrogression forming of AA7075-T6 is recommended at 200 °C, strain rates up to at least 10⁻¹ s⁻¹, and total processing times within 3 to 12 minutes. Forming under these conditions can provide sufficient ductility to produce automotive structural components of reasonable geometric complexity, as was recently demonstrated. [28,29] The true flow stress in AA7075-T6 predicted by Eq. [5] at 200 °C and a true-strain rate of 10^{-1} s⁻¹ is 402 MPa, which is in good agreement with the tensile data in Table V. This true flow stress is 21 pct less than the mean YS of the T6 temper at room temperature. Retrogression forming at these recommended conditions will reduce the force required to form components and reduce springback compared to forming at room temperature. At 200 °C and a true-strain rate of 10^{-1} s⁻¹, both e_r and RA are nearly double those of the T6 temper at room temperature. The small strain-rate sensitivity of

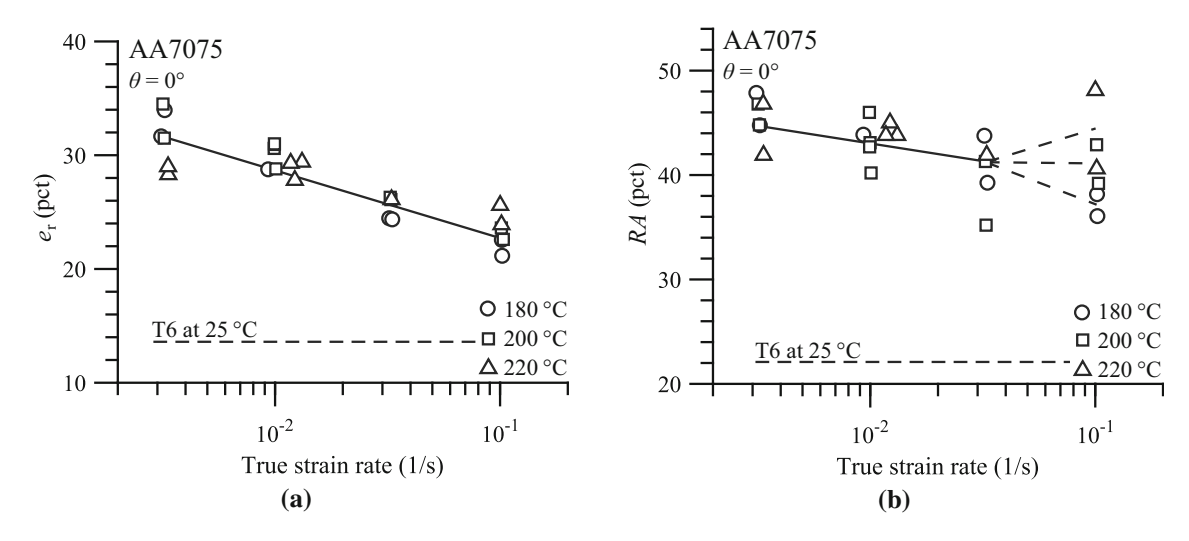


Fig. 9—(a) Tensile elongation (e_r) and (b) reduction in area (RA) are plotted as functions of true-strain rate on a logarithmic scale for specimens of AA7075 in the $\theta=0$ deg orientation. Specimens were tested at 180, 200, and 220 °C. Average values for the T6 temper at room temperature are indicated by horizontal dashed lines.

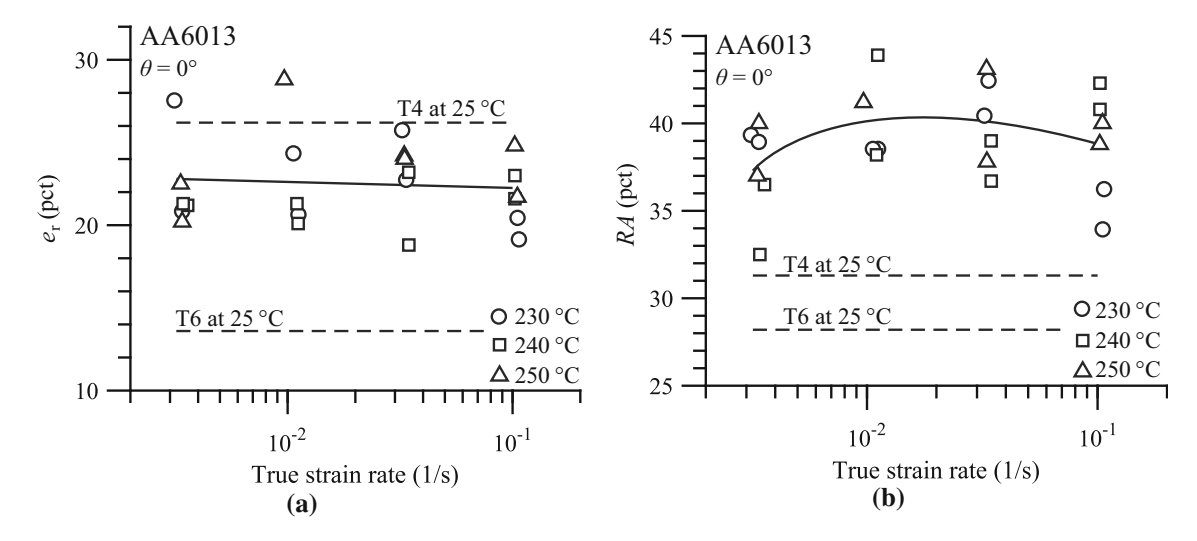


Fig. 10—(a) Tensile elongation (e_r) and (b) reduction in area (RA) are plotted as functions of true-strain rate on a logarithmic scale for specimens of AA6013 in the $\theta=0$ deg orientation. Specimens were tested at 230 °C, 240 °C, and 250 °C. Average values for the T4 and T6 tempers are indicated by horizontal dashed lines.

m=0.039 at elevated temperatures suggests that tensile ductility is improved primarily by delaying fracture, not by delaying neck development. [3,48,52-55] Previous studies on the warm formability of AA7075-T6 also recommended forming at or near 200 °C. [1,2,9-12] For example, Wang *et al.* determined that AA7075-T6 has the best deep drawing performance near 180 °C and the best stretch formability near 220 °C. [9] Time at temperature produces no effect on the forces required to deform AA7075-T6, as demonstrated in Figure 6. This suggests that the flow stresses at these warm temperatures do not depend on the finest precipitates, which dissolve during retrogression, but may depend primarily on the largest precipitates. For the recommended conditions, true flow stress, tensile elongation, and reduction in area do not vary significantly with specimen orientation relative to sheet rolling direction. Reaging with a simulated paint-

bake heat treatment should increase strength after retrogression forming, though it is not as effective as reaging with a recommended reaging heat treatment. Preliminary results from retrogression forming and reaging experiments with a similar sheet material suggest that reaging with the paint bake alone after significant deformation might restore T6 strength. [28] These results differ from the results of the present study, which applied a simulated paint-bake heat treatment after a retrogression heat treatment without plastic deformation.

Retrogression forming of AA6013-T6 is recommended at 240 °C, strain rates up to at least 10^{-1} s⁻¹, and total processing times no longer than 7 minutes. The true flow stress in AA6013-T6 predicted by Eq. [5] at 240 °C and a true-strain rate of 10^{-1} s⁻¹ is 292 MPa, which is in good agreement with the tensile data in

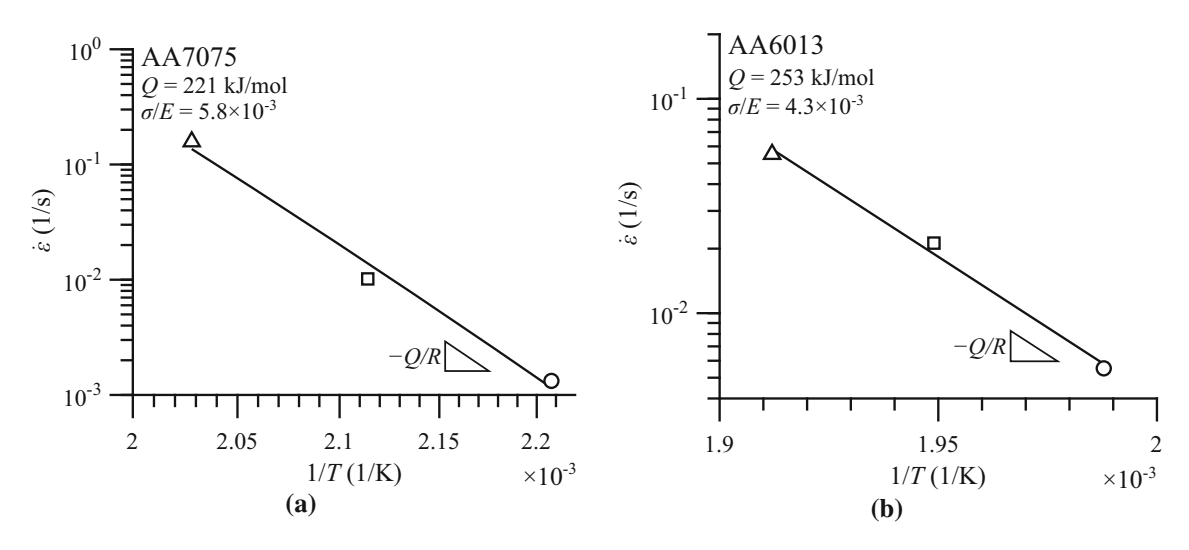


Fig. 11—The activation energy for plastic flow is measured for (a) AA7075 and (b) AA6013 from plots of true-strain rate at a constant σ_{10}/E against the inverse of absolute temperature on dual-logarithmic scales.

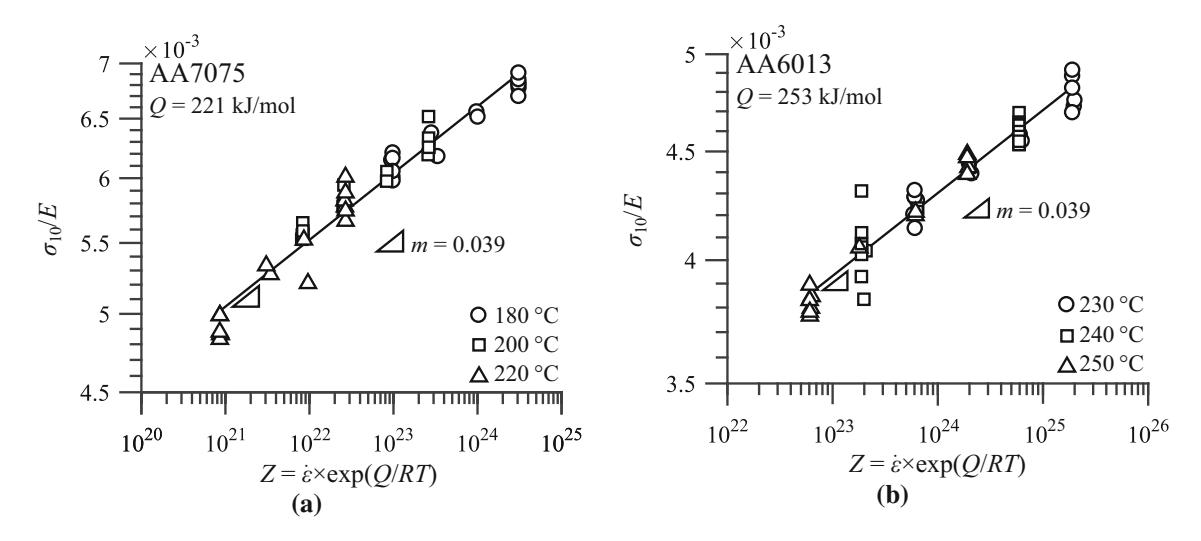


Fig. 12—Flow stress at a plastic true strain of 0.10, normalized by the temperature-dependent dynamic unrelaxed Young's modulus [14,37] (σ_{10}/E) is plotted as a function of the Zener–Hollomon parameter (Z) for (a) AA7075 and (b) AA6013 on dual-logarithmic scales. The slope of the data is the strain-rate sensitivity (m).

Table V. While this true flow stress is 40 pct greater than the mean room-temperature YS of the T4 temper (210 ± 9 MPa), it is 17 pct less than σ_{10} at room temperature for the T4 temper (352 ± 6 MPa). Retrogression forming of AA6013-T6 at the recommended conditions requires less force than room-temperature forming in the T6 temper and may require less force than room-temperature forming in the T4 temper at large strains. At 240 °C and a true-strain rate of 10^{-1} s⁻¹, $e_{\rm r}$ is 1.6 times that of the T6 temper and 0.8 times that of the T4 temper at room temperature. At these same conditions, RA is 1.5 times that of the T6 temper and 1.4 times that of the T4 temper at room temperature. Considering these results, retrogression forming AA6013-T6 at the recommended conditions might match the formability of the T4 temper

at room temperature but will produce higher strengths than formed T4 material. For the recommended conditions, true flow stress, tensile elongation, and reduction in area do not vary significantly with specimen orientation relative to the sheet rolling direction. Reaging AA6013 with a simulated paint bake is just as effective as reaging with the recommended reaging heat treatment of 190 °C for 1 hour. Therefore, AA6013 is well suited for using the automotive paint bake as surrogate for the reaging heat treatment. However, retrogression forming AA6013-T6 is expected to only modestly improve formability, especially when compared to the expected formability of AA6013-T4 sheet at room temperature. Therefore, AA6013 sheet material is not as well suited for retrogression forming and reaging as AA7075 sheet.

V. CONCLUSIONS

The mechanical behaviors of AA7075-T6 and AA6013-T6 sheet materials were evaluated using uniaxial tensile tests at temperatures (180 to 220 °C for AA7075-T6 and 230 to 250 °C for AA6013-T6) and true-strain rates (3×10^{-3} to 10^{-1} s⁻¹) suitable to retrogression forming. Room-temperature tensile properties were evaluated in several heat-treated conditions pertinent to the retrogression forming and reaging (RFRA) process. The data obtained were used to define conditions suitable to retrogression forming and to predict the tensile behaviors of the materials under those conditions. The following conclusions were reached.

- 1. Retrogression forming of AA7075-T6 is recommended at 200 °C, true-strain rates up to at least 10⁻¹ s⁻¹, and total processing times within 3 to 12 minutes. Under these conditions, tensile elongation is 1.8 times that of the T6 temper at room temperature, and reduction in area is 1.8 times that of the T6 temper at room temperature.
- 2. Retrogression forming of AA6013-T6 is recommended at 240 °C, true-strain rates up to at least 10^{-1} s⁻¹, and total processing times no longer than 7 minutes. Under these conditions, tensile elongation is 0.8 times that of the T4 temper and 1.6 times that of the T6 temper at room temperature. Reduction in area is 1.4 times that of the T4 temper and 1.5 times that of the T6 temper at room temperature.
- 3. Neither AA7075 nor AA6013 exhibit significant strain hardening under tensile deformation at the elevated temperatures studied, 180 to 220 °C for AA7075 and 230 to 250 °C for AA6013. Instead, an approximately steady-state true flow stress is observed at constant temperature and constant truestrain rate.
- 4. The activation energy of plastic flow for AA7075 at temperatures from 180 to 220 °C and true-strain rates from 3.2×10^{-3} to 10^{-1} s⁻¹ is 221 kJ/mol.
- 5. The activation energy of plastic flow for AA6013 at temperatures from 230 to 250 °C and true-strain rates from 3.2×10^{-3} to 10^{-1} s⁻¹ is 253 kJ/mol.
- 6. The average strain-rate sensitivity of both AA7075 and AA6013 across the elevated temperatures and true-strain rates investigated is m = 0.039.
- 7. The values measured for activation energy and strain-rate sensitivity are used to produce models, based on Eqs. [2] and [5], that predict flow stress as a function of temperature and true-strain rate for both AA7075 and AA6013 across the elevated temperatures and true-strain rates examined in this study.
- 8. Extended soaking times of up to 900 s at 200 °C prior to tensile deformation at $\dot{\varepsilon} = 8 \times 10^{-2} \text{ s}^{-1}$ do not affect the flow stress of the AA7075 material. This suggests that flow behavior at 200 °C is controlled by the largest precipitates, which do not dissolve during a retrogression heat treatment.
- 9. The flow behaviors and tensile ductilities of both AA7075 and AA6013 are generally isotropic within

the sheet plane at temperatures suitable to retrogression forming.

ACKNOWLEDGMENTS

The authors thank Dominic Fascitelli, Brent Mobbs, Daniel Nikolai, Tucker Roemer, and Matthew Schick for their assistance in obtaining tensile data. This work was supported by the National Science Foundation under GOALI grant number CMMI-1634495. One author, K. E. Rader, expresses gratitude to General Motors for support during summer research activities.

CONFLICT OF INTEREST

On behalf of all authors, the corresponding author states that there is no conflict of interest.

REFERENCES

- R.S. Long, E. Boettcher, and D. Crawford: *JOM*, 2017, vol. 69 (12), pp. 2635–39.
- K. Zheng, D.J. Politis, L. Wang, and J. Lin: *Int. J. Light. Mater. Manuf.*, 2018, vol. 1 (2), pp. 55–90.
- L. R. Morris and R. A. George: SAE Tech. Pap. Ser., 1977, no. 770206.
- 4. P. E. Krajewski: SAE Tech. Pap. Ser., 2006, no. 2006-01-0984.
- 5. N.R. Harrison and S.G. Luckey: SAE Int J. Mater. Manuf., 2014, vol. 7 (3), pp. 567–573.
- A. Keci, N. R. Harrison, and S. G. Luckey: SAE Tech. Pap. Ser., 2014, no. 2014-01-0984.
- J. Mendiguren, E.S. de Argandona, and L. Galdos: IOP Conf. Ser. Mater. Sci. Eng., 2016, vol. 159, p. 012016.
- W. Xiao, B. Wang, and K. Zheng: Int. J. Adv. Manuf. Tech., 2017, vol. 92, pp. 3299–309.
- H. Wang, Y. Luo, P. Friedman, M. Chen, and L. Gao: Trans. Nonferr. Met. Soc. China, 2012, vol. 22, pp. 1–7.
- W. Huo, L. Huo, Y. Zhang, and J. Zhang: *Mater. Sci. Eng. A*, 2016, vol. 675, pp. 44–54.
- 11. H. Kim, L. Cronley, C. Reichert, and P. Zelenak: *Int. Auto. Body Cong.*, 2017, vol. 20, pp. 1–11.
- H. Kim, R. Hagnlen, T. Feister, and V. Tunga: *IOP Conf Ser. Mater. Sci. Eng.*, 2018, vol. 418 (012029), pp. 1–8.
- T.A. Ivanoff, J.T. Carter, L.G. Hector, Jr, and E.M. Taleff: *Metall. Mater. Trans. A*, 2019, vol. 50 (3), pp. 1545–61.
- E.M. Taleff, P.J. Nevland, and P.E. Krajewski: *Metall. Mater. Trans. A*, 2001, vol. 32 (5), pp. 1119–30.
- ASM Handbook Committee: ASM Handbook, Volume 2: Properties and Selection: Nonferrous Alloys and Special-Purpose Materials, ASM International, Materials Park, OH, 1990, pp. 62-122.
- K. Anderson, J. Weritz, and J. G. Kaufman (eds.): ASM Handbook, Volume 2B: Properties and Selection of Aluminum Alloys, 2019, pp. 432-438.
- 17. M. B. Kannan, P. B. Srinivasan, and V. S. Raja: *Stress Corrosion Cracking*, Woodhead Publishing, 2011, pp. 307-340.
- 18. J.P. Immarigon, R.T. Holt, A.K. Koul, L. Zhao, W. Wallace, and J.C. Beddos: *Mater. Char.*, 1995, vol. 35, pp. 41–67.
- N.C. Danh, K. Rajan, and W. Wallace: *Metall Trans. A*, 1983, vol. 14 (9), pp. 1843–1850.
- 20. Alcoa Inc.: Alcoa Technical Fact Sheet: Alloy 6013 sheet: Maximum Strength 6xxx Series Sheet, Alcoa Inc., Bettendorf, Iowa, 2017.
- 21. V. Burt: ASM Handbook, Volume 2A: Aluminum Science and Technology, 2018, pp. 336–356.
- 22. M. Kumar and N.G. Ross: *J. Mater. Process. Tech.*, 2016, vol. 231, pp. 189–98.
- 23. M. Aumüller: AluReport, 2014, vol. 24, pp. 14–15.

- 24. K.E. Rader, T.A. Ivanoff, H. Shin, J. Carter, L.G. Hector, Jr, and E.M. Taleff: Light Metals, 2018, vol. 2018, pp. 241-46.
- 25. K.E. Rader, J. Carter, L. Hector, Jr, and E.M. Taleff: Light Metals, 2019, vol. 2019, pp. 159-64.
- 26. K.E. Rader, M. Schick, J. Carter, L. Hector, Jr, and E.M. Taleff: Light Metals, 2019, vol. 2019, pp. 187-91.
- 27. K.E. Rader, J. Carter, L. Hector, Jr, and E.M. Taleff: Light Metals, 2020, vol. 2020, pp. 400-05.
- 28. K.E. Rader, J. Carter, L. Hector, Jr, and E.M. Taleff: Light Metals, 2020, vol. 2020, pp. 247-52.
- 29. K. E. Rader, J. Carter, L. Hector, Jr., and E. M. Taleff: Light Metals, 2021.
- 30. K. E. Rader, J. Carter, L. Hector, Jr., and E. M. Taleff: Metall. Mater. Trans. A, 2021.
- 31. J.K. Park and A.J. Ardell: Metall. Trans. A, 1984, vol. 15, pp. 1531-43.
- 32. Alcoa Inc.: Alcoa Technical Fact Sheet: Alloy 7075 Plate and Sheet, Alcoa Inc., Bettendorf, Iowa, 2017.
- 33. ASTM E8: ASTM International, West Conshohocken, PA, 2017.
- 34. ASTM E2448: ASTM International, West Conshohocken, PA, 2017.
- 35. ASTM E385-17: ASTM International, West Conshohocken, PA,
- 36. ASTM E6: ASTM International, West Conshohocken, PA, 2017.
- 37. V.W. Köster: Zeitschrift fut Metall., 1948, vol. 39, pp. 1–12.
- 38. R.N. Lumley, A.J. Morton, R.G. O'Donnell, and I.J. Polmear: Heat Treat Prog., 2005, vol. 5 (2), pp. 23-29.
- 39. L. Zhuang, R. de Haan, J. Bottema, C.T.W. Lahaye, and P. De Smet: *Mater. Sci. Forum*, 2000, vol. 331–337, pp. 1309–14. 40. D.C. Balderach, J.A. Hamilton, E. Leung, M.C. Trejeda, J. Qiao,
- and E.M. Taleff: Mater. Sci. Eng. A, 2002, vol. 339, pp. 194-204.

- 41. J.H. Hollomon: Trans. AIME, 1945, vol. 162, pp. 268-90.
- 42. The MathWorks, Inc.: MATLAB [Software], Version R2016b, 2016, Available from https://www.mathworks.com/ products/matlab.
- 43. O.G. Sherby and P.M. Burke: Prog. Mater. Sci., 1968, vol. 13, pp. 325-90.
- 44. M.E. Kassner: Fundamentals of Creep in Metals and Alloys, 3rd ed., Butterworth Heinemann, Waltham, 2015.
- 45. O.D. Sherby, R.L. Orr, and J.E. Dorn: Trans. AIME, 1954, vol. 1954, pp. 71-80.
- 46. J.J. Jonas, C.M. Sellars, W.J. McG, and W.J.Mc.G. Tegart: Metall. Rev., 1969, vol. 14 (1), pp. 1-24.
- 47. E.U. Lee, H.H. Kranzlein, and E.E. Underwood: Mater. Sci. Eng., 1971, vol. 7 (6), pp. 348-56.
- 48. T.G. Langdon: Metall. Trans. A, 1982, vol. 13, pp. 689-701.
- 49. J. Noder: Master's Thesis, 2017, Univ. of Waterloo, Canada.
- 50. H. Rong, P. Hu, L. Ying, W. Hou, and J. Zhang: Int. J. Mech. Sci., 2019, vol. 156, pp. 59-73.
- 51. C. Zener and J.H. Hollomon: J. Appl. Phys., 1944, vol. 15 (1), pp. 22-32.
- 52. D.A. Woodford: Trans. ASM, 1969, vol. 62, pp. 291-93.
- 53. M.A. Burke and W.D. Nix: Acta Metall., 1975, vol. 23, pp. 793–98.
- 54. J.W. Hutchinson and H. Obrecht: Fracture, 1977, vol. 1, pp. 101-16.
- 55. J.W. Hutchinson and K.W. Neale: J. Mech. Phys. Solids, 1983, vol. 31 (5), pp. 405-26.

Publisher's Note Springer Nature remains neutral with regard to jurisdictional claims in published maps and institutional affiliations.